Supplement: Glacier damage evolution over ice flow timescales

Meghana Ranganathan[1,2], Alexander Robel[2], Alexander Huth[3], and Ravindra Duddu[4]

[1]University Corporation for Atmospheric Research, Boulder, CO, USA
[2]School of Earth and Atmospheric Sciences, Georgia Institute of Technology, Atlanta, GA, USA
[3]Geophysical Fluid Dynamics Laboratory, Princeton, NJ, USA
[4]School of Engineering, Vanderbilt University, Nashville, TN, USA

Correspondence: Meghana Ranganathan (meghanar@ucar.edu)

1 Coupled Flowline/Damage Model

1.1 Flowline Model and Numerical Implementation

In Section 2 of the main text, we implement a flowline model initially posed in Schoof (2007) and used in previous studies, including Robel et al. (2014) and Christian et al. (2022). These studies have described this model in significant detail and thus can be used to supplement any detail not outlined here.

This model implements a one-dimensional form of the momentum and mass balance equations:

$$\rho_{\mathrm{i}} g h \frac{\partial s}{\partial x} = \frac{\partial}{\partial x}\left[2hA^{-1/n}\left|\frac{\partial u}{\partial x}\right|^{\frac{1}{n}-1}\frac{\partial u}{\partial x}\right] - C|u|^{m-1}u \tag{1}$$

$$\frac{\partial h}{\partial t} = \dot{a} - \frac{\partial(uh)}{\partial x} \tag{2}$$

in which u, h, s are ice velocity, thickness, and surface elevation, respectively. The parameters are: ρ_{i} is the density of ice, g is the gravitational constant, A is the flow-rate parameter, n is the stress exponent is Glen's flow law, C is the sliding coefficient, m is the sliding exponent, $\dot{a}$ is the surface accumulation rate.

The glacier terminates at the grounding line, with no ice shelf, and therefore the thickness boundary condition at the end of the domain is

$$h_L = -\frac{\rho_{\mathrm{w}}}{\rho_{\mathrm{i}}}b(x_g) \tag{3}$$

where L is the length of the glacier, ρ_{w} is the density of water, b is the bed elevation measured from sea level, and x_g is the grounding line position. At the terminus, the velocity is found by

$$\rho_{\mathrm{i}} g h_L(1 - \frac{\rho_{\mathrm{i}}}{\rho_{\mathrm{w}}}) = \frac{\partial}{\partial x}\left[2hA^{-1/n}|\frac{\partial u}{\partial x}|^{\frac{1}{n}-1}\frac{\partial u}{\partial x}\right] \tag{4}$$

To solve for velocity and thickness, we follow the implementation outlined in Schoof (2007). As the grounding line advances and retreats, the grid in the x-direction is allowed to stretch and contract. To allow for this, we rescale the $x-$coordinates to

1

20 define a new coordinate variable γ, where $\gamma = 0$ describes the inflow boundary and $\gamma = 1$ describes the terminus. Note that in previous work, this parameter was denoted as σ, but to avoid confusion with stress in this work, we denote this γ.

We solve Equations 1, 2 using an implicit finite difference scheme, in which the derivatives in the x-direction are approximated by an upwind scheme. There are two differences between the implementation here and the one outlined in Schoof (2007). First, as in Christian et al. (2022), we force the model with frontal melt forcing such that the thickness approximation

25 at the terminus becomes

$$0 = \frac{h_i^k - h_i^{k-1}}{\Delta t} - \frac{\gamma}{x_g}\frac{(x_{g_i}^k - x_{g_i}^{k-1})(h_i^k - h_{i-1}^k)}{\Delta t \Delta \gamma} + \frac{(h_i^k(u_i^k + \dot{m}\frac{h_f}{h_i^k} + u_{i-1}^k) - h_{i-1}^l(u_{i-1}^k + u_{i-2}^k)}{2x_{g_i}^k \Delta \gamma} - \dot{a} \tag{5}$$

in which there is an extra term in the $\frac{\partial(uh)}{\partial x}$ approximation to account for frontal melt forcing at the terminus. Second, in order for viscosity to vary with damage, we let viscosity vary spatially over the grid. We do this through the parameter ϵ defined in Schoof (2007) to represent ice viscosity. We scale this such that $\tilde{\epsilon} = \epsilon(1 - D)^{-1/n}$, where ϵ is as defined in Schoof (2007) and

30 $\tilde{\epsilon}$ is used in its stead in this work.

1.2 Transient Damage Model and Numerical Implementation

In Section 2.2, we implement a transient damage model based on Pralong and Funk (2005) to compare against our diagnostic damage model:

$$\frac{\partial D^*}{\partial t^*} + u^*\frac{\partial D^*}{\partial x^*} = \delta(\tilde{\sigma}^*_x - \sigma_t^*)^r(1-D)^{-k} \tag{6}$$

35 where all parameters here are nondimensionalized as described in Section 2.1 of the main text. Here, D is damage, u is ice velocity, δ is the nondimensional parameter describing the ratio of advective to fracture timescales, $\tilde{\sigma}^*_x$ is the effective maximum principal stress, σ_t^* is the nondimensional stress threshold, r, k are material parameters.

To find the source term f in the one-dimensional flowline model, we first determine σ_x as

$$\sigma_x = \frac{3}{2}\tau_x - \frac{1}{2}\rho_i g(h - z) \tag{7}$$

40 $$\tau_x = 2\eta\frac{\partial u}{\partial x} \tag{8}$$

$$\eta = A\left[\sqrt{\frac{1}{2}\left(\frac{\partial u}{\partial x}\right)^2}\right]^{\frac{1-n}{n}} \tag{9}$$

where τ_x describes the longitudinal deviatoric stress, z is the vertical coordinate, and η is the dynamic viscosity. We then convert the x-coordinates to γ as described above.

We solve the damage equation using an upwind scheme to approximate the $x-$ derivatives as follows:

45 $$\frac{\partial(uD)}{\partial \gamma} \approx \frac{D_i^k(u_i^k + u_{i-1}^k) - D_{i-1}^k(u_{i-1}^k + u_{i-2}^k)}{2\Delta \gamma} \tag{10}$$

The ice enters the inflow boundary undamaged and is allowed to advect out of the outflow boundary.

2   Diagnostic Damage Model: Other Melt Scenarios

In the main text, we test the diagnostic damage model against different climate forcing scenarios that may affect the flow timescale of the model. Here, we show other scenarios not presented in the main text (Figure S1). We first test annual melt forcing with a smaller degree of variability than shown in the main text, in which the error in grounding line position is lesser than the annual forcing example presented in the main text. We also present an interannual variability example, in which frontal melt forcing oscillates in a 7-year cycle. This produces a similar degree of error in the grounding line position as annual melt forcing. Finally, we test a constant frontal melt forcing of $\mu_m = 100$ m yr^{-1}, a much higher rate of melt than presented in the main text. Even with a significant increase in the melt rate, the diagnostic damage solver reproduces the grounding line change of the transient model with a smaller error ($< 5\%$ by 1000 years).

Given these results, we would expect that for a large frontal melt forcing and a large degree of variability on short timescales, the diagnostic damage solver would produce a larger error than with smaller melt forcing or degree of variability. However, the results here suggest that, for physical scenarios, the diagnostic damage solver should produce reasonable damage estimates and, thus, similar ice sheet response as the full transient damage models.

3   Validation of Diagnostic Damage Model in MISMIP+ Simulation

We validated the diagnostic damage model using a flowline model in the main text. Here, we validate the MISMIP+ simulations against the transient creep damage model in Pralong and Funk (2005) (Figure S2). We apply the same parameters from Huth et al. (2021), but in the isotropic damage formulation described in Pralong and Funk (2005). The error between the diagnostic and transient model is less then 0.15% over 100 years. There are minor differences in the damage field, particularly at the calving front in the center of the domain, though these differences do not appear to have a significant effect on the flow response.

We also validate the model in a two-dimensional simulation against previous studies that have applied transient damage models to the MISMIP+ simulation (Figure S3). Huth et al. (2021) applies a version of the model derived by Pralong and Funk (2005) to represent calving and rift propagation in ice shelves. They demonstrate the model using the MISMIP+ geometry, and they run the coupled flow and damage model to 0.06 years and 0.2 years (Figure S3b). They find that two lobes of elevated damage develop in the glacier margins just downstream of the grounding line after ~ 0.5 years, which is similar to the damage structure we find when running the diagnostic damage model for 0.5 years. Their simulation also captures a sharp rift that propagates across the domain and connects the two lobes of elevated damage; however, our diagnostic model developed for decadal to century-scale applications does not capture this sharp rifting. Further, we estimate more damage in the trunk of the ice shelf, near the terminus. This is likely because we apply basal melt forcing on the ice shelf, which Huth et al. (2021) does not.

We next compare our damage estimates to that of Sun et al. (2017), which applies a transient damage model to the full MISMIP+ scenario in which they initiate basal melt forcing and run the model for 100 years. Given the duration of this model, we compare their damage estimates to our damage estimates after spinning up to steady state with damage and then running
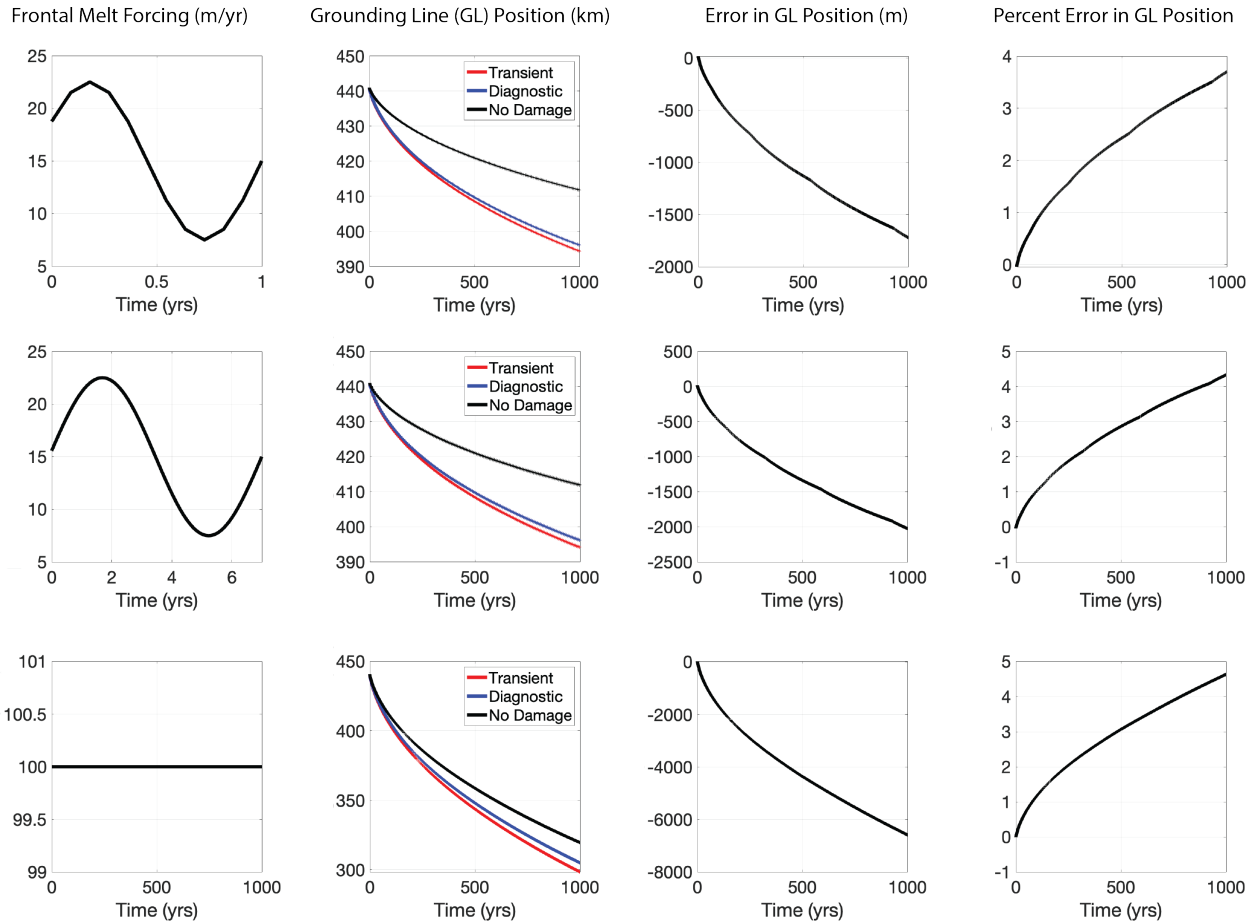
Figure S1. Similar to Fig. 3 in the main text. We run three different model simulations using no damage coupling, the full transient damage model of Pralong and Funk (2005), and the diagnostic damage model. We present the melt forcing (column 1), grounding line position (column 2), the absolute error in grounding line position between the diagnostic damage model and the transient damage model, and the error in grounding line position as a percent of the amount of grounding line retreat by the transient model: (top row) annual frontal melt variability with a lower fraction of variability, (middle row) interannual frontal melt forcing, (bottom row) Constant frontal melt forcing with a higher rate of melt.
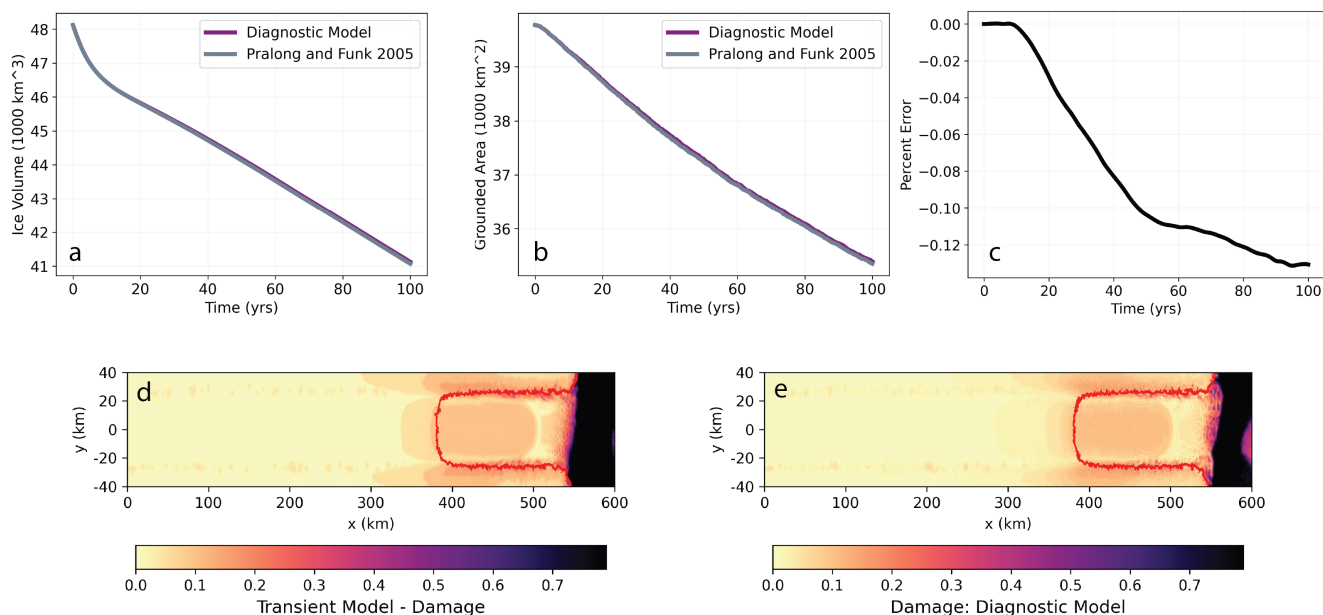
Figure S2. Comparison of our damage estimates to those of the transient Pralong and Funk (2005) model applied to the same model geometry: (a) ice volume over 100 years and (b) grounded area over 100 years with both the diagnostic and transient models, (c) percent error between the transient and diagnostic models, as a percent of the transient model output, (d) damage field after 100 years using the transient model, (e) damage field after 100 years using the diagnostic model.

the coupled flow and damage model for 100 years in response to basal melt forcing. They find damage across the ice shelf, primarily concentrated along the margins and with elevated damage near the terminus in the trunk of the ice shelf (Figure S3d). We find a similar damage field, in which there is significant damage accumulation in the margins and some damage in the trunk of the ice shelf near the terminus (Figure S3c). There is a minor difference in the center of the ice shelf near the grounding line, in which we find a circular region of elevated damage where they find damage to taper off with proximity to the grounding line.

4 Converting Deviatoric to Cauchy Stresses

We calculate damage in 3D in order to capture the effect of overburden pressure counteracting the opening of cracks. However, the ice flow model icepack operates using the shallow-stream approximation, which captures ice flow in two dimensions and assumes that velocity is constant with depth. Therefore, to calculate 3D damage, we compute deviatoric stresses from the flow model and convert the deviatoric stresses to Cauchy stresses, following the previous work of Keller and Hutter (2014); Huth

Comparison to Huth et al. 2021b

(a) Diagnostic Damage after 0.25 years
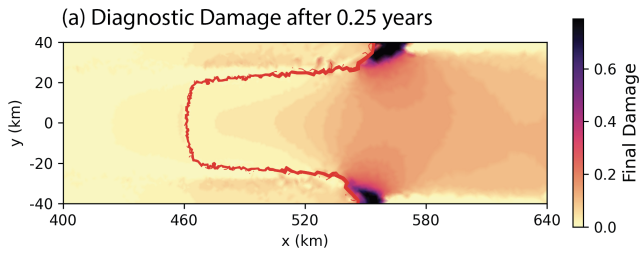
(b) Huth et al. 2021b after 0.06, 0.2, 0.486 years
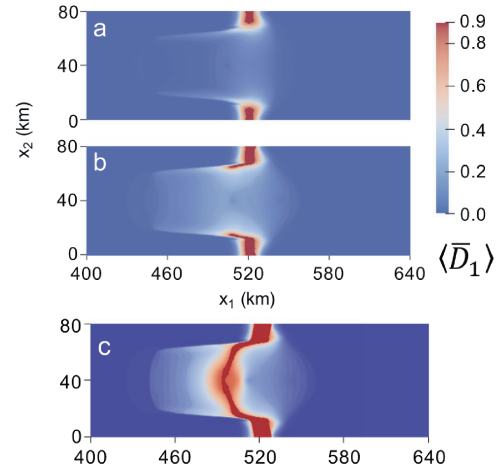
Adapted from Huth et al. 2021b, Fig 2-3

Comparison to Sun et al. 2017

(c) Diagnostic Damage after 100 years
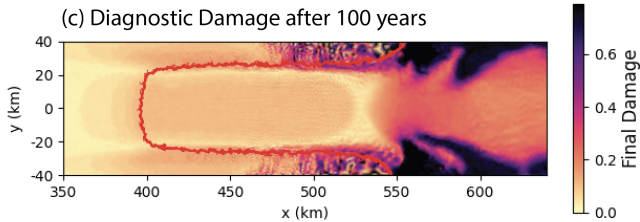
(d) Sun et al. 2017 after 100 years

t = 100 a
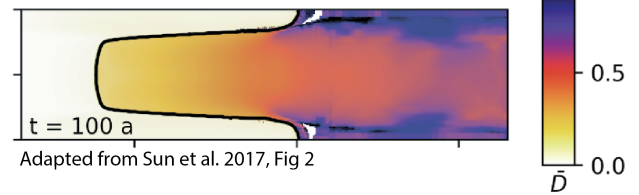
Adapted from Sun et al. 2017, Fig 2

Figure S3. Comparison of our damage estimates to those of transient damage models applied to the MISMIP+ experimental setup. (a-b) We compare our estimates to that of Huth et al. (2021), which used the MISMIP+ geometry to simulate rifting and calving on short timescales. (c-d) We compare our estimates to that of Sun et al. (2017), which used the MISMIP+ experiments to estimate the effect of damage on flow over century timescales.

et al. (2021) as

$$\sigma_{ij} = \tau_{ij} - p\delta_{ij} \tag{11}$$

where σ_{ij} is the Cauchy stress tensor, τ_{ij} is the deviatoric stress tensor, p is pressure, and δ_{ij} is the Kronecker delta.

The choice of pressure p affects where we allow damage to accumulate. In this study, we set $p = p_{\mathrm{i}}$, ice overburden pressure, which is

$$p_{\mathrm{i}} = \rho_{\mathrm{i}} g(h - z) - \tau_{xx} - \tau_{yy} \tag{12}$$

where ρ_{i} is ice density, g is the gravitational constant, h is ice thickness, z is the vertical coordinate, and τ_{xx}, τ_{yy} are the in-plane deviatoric normal stresses. The pressure is therefore monotonically increasing with depth, producing damage that accumulates primarily at the surface. However, in regions of the glacier in which the base of the ice is in contact with water, such as on ice shelves or in grounded ice that flows over subglacial channels, water pressure can counteract the ice overburden pressure, allowing for damage accumulation at the base of ice shelves and glaciers. As outlined in Keller and Hutter (2014); Huth et al. (2021), this can be modeled through the use of an effective pressure in Equation 11, in which

$$p_{\mathrm{eff}} = \begin{cases} 0 & z \geq z_{\mathrm{sl}} \\ \rho_{\mathrm{w}} g(z_{\mathrm{sl}} - z) & z < z_{\mathrm{sl}} \end{cases} \tag{13}$$

where z_{sl} is the height of sea level and is set to $z_{\mathrm{sl}} = 0$ as in Huth et al. (2021), and ρ_{w} is the density of seawater. In the next section, we describe how including this effective pressure would increase the magnitude of damage estimated at each timestep and therefore enhance the overall effect of damage on flow.

5 Basal crevassing

In Figure S4, we evaluate the effects of including basal crevassing on our results. We calculate damage using the diagnostic model at steady-state in the MISMIP+ configuration, calculating Cauchy stresses using just ice overburden pressure (Figure S4a) and using effective pressure (Figure S4b). For each case, we show vertical slices through the glacier of the Hayhurst stress (Figure S4i,iii) and the damage field (Figure S4ii,iv), in which the slices are taken through the margin (Figure S4i,ii) and through the centerline (Figure S4iii,iv). We set the stress threshold to be $\sigma_t = 0.2\,\mathrm{MPa}$.

If using ice pressure (Figure S4a), the Hayhurst stress is largest at the surface and smaller at depth, due to depth varying compressive (negative) ice pressure. The stress also is larger downstream of the glacier than upstream, with the smallest stress being upstream near the bed. In the margin slice, there is a minimum in stress through the ice column right at the grounding line. Damage is set to $D = 1$ where the Hayhurst stress exceeds the stress threshold $\sigma_t = 0.2\,\mathrm{MPa}$. There are small amounts of damage concentrated at the surface in both the margin and the centerline, with damage extending deeper through the ice column in the margin slice.

WhenIf using effective pressure (Figure S4b), the Hayhurst stress is larger on the ice shelf at depth than in the ice pressure case, due to the effects of water pressure in basal crevasses. The difference in the margin is more minor, since damage in the
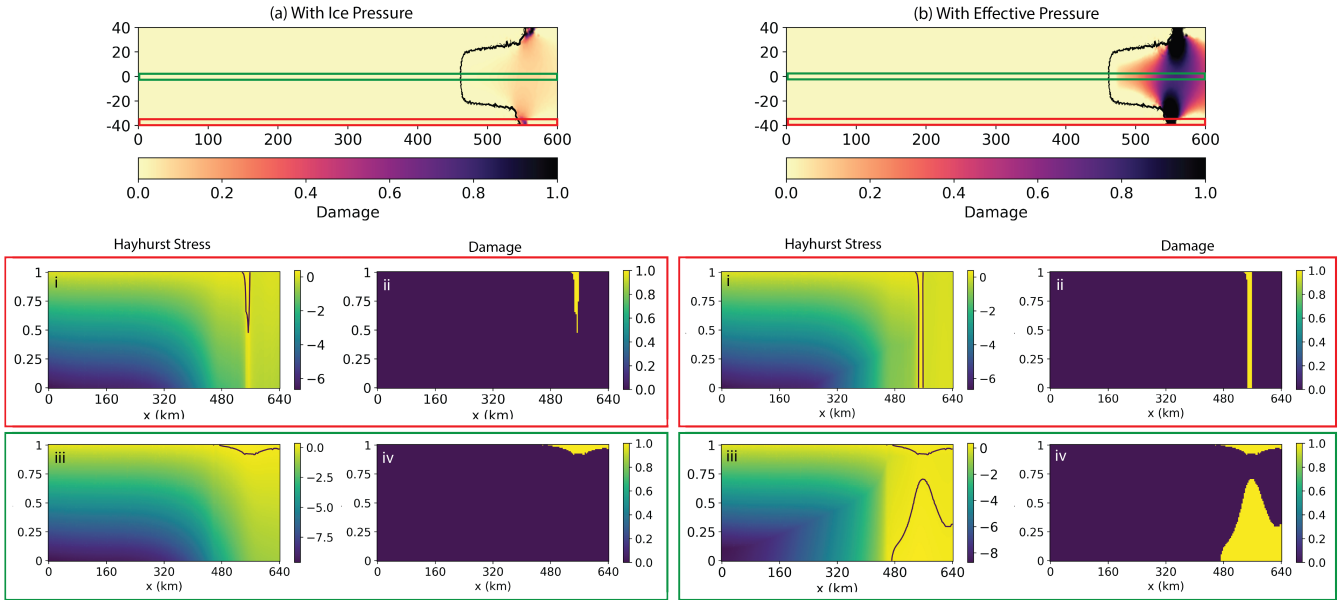
Figure S4. Including basal crevassing: Calculations of Hayhurst stress and damage using (a) ice pressure and (b) effective pressure to calculate Cauchy stresses from deviatoric stresses. For each case, we show the 2D damage field calculated using the diagnostic model from the steady-state MISMIP+ configuration. We also show vertical slices through the margin of (i) Hayhurst stress and (ii) damage and vertical slices through the centerline of (iii) Hayhurst stress and (iv) damage. Contours on the Hayhurst stress fields show where the stress is 0.2 MPa, the stress threshold.

margins is concentrated into two lobes at the grounding line. However, the stress in that lobe is high enough to produce damage through the full ice thickness, so $\bar{D} = 1$ in the margin. In the centerline on the ice shelf, the Hayhurst stress is higher at depth than in the ice pressure case. Along the bulk of the ice shelf centerline, there are regions of $\sigma \geq \sigma_t$ (Figure S4b,iii), producing a region of damage at the base of the ice shelf along with a region of damage at the surface (Figure S4b,iv).

125   As a result, the depth-averaged damage using effective pressure (Figure S4b) is much higher than the depth-averaged damage using ice pressure (Figure S4a). Therefore, using effective pressure in the results here would likely further enhance the effects of damage on flow.

6   Timestep and Mesh Size Dependence of Diagnostic Damage Model

Here we show the sensitivity to mesh size and timestep of the diagnostic damage model. We initialize these simulations with a
130   steady-state MISMIP+ configuration with no damage, and we run the simulations with no external forcing in order to identify
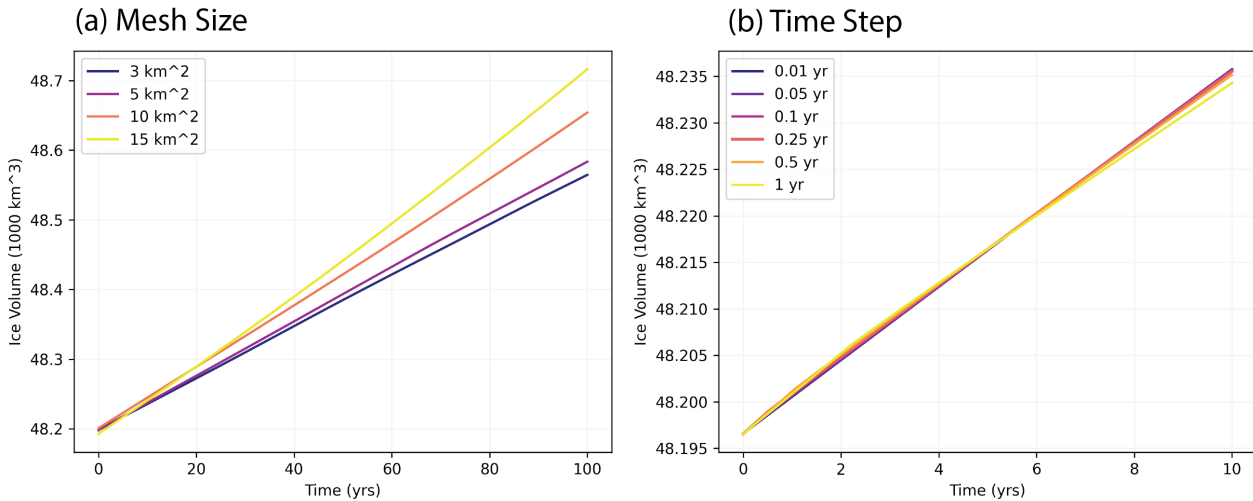
Figure S5. Evaluating the (a) mesh size and (b) timestep dependence of the diagnostic damage model, in the MISMIP+ geometry, initialized with no damage and run with no basal melting.

the mesh size and timestep dependence of only the damage model. Because there is no external (basal melt) forcing, damage causes ice volume to increase slightly over the simulation period, as the steady state with damage has a slightly larger mass than the steady state without damage.

To evaluate the effect of mesh size (Figure S5a), we create a mesh with triangular elements of the same area across the domain and vary the element sizes from $3-15 \text{ km}^2$. In general, as mesh size increases, the change in ice volume also increases, because as mesh size increases, damage is applied over a larger area of the glacier. However, as the mesh size decreases, the effect of mesh size also decreases; the difference between 3 and 5 km^2 is very small after 100 years. While here, we test mesh sizes that are applied uniformly across the domain, in the basal melt simulations we use a mesh that is refined near the grounding line, where the melt is being applied. The mesh size begins at 8 km^2 away from the grounding line and reduces to 1 km^2 at the grounding line quadratically with proximity to the grounding line.

To evaluate the effect of timestep (Figure S5b), we run simulations for 10 model-years with varying timesteps from 0.01 year to 1 year. The effect of timestep within these bounds is very small. In the main text, we use a timestep of $\Delta t = 0.25$ year.

7 Effect of D_{max}

In the study, we take the value of $D_{\text{max}} = 0.79$ for numerical convergence reasons. Larger values of D_{max} produce viscosity values close to zero and, thus, cause difficulties with convergence of the flow solver. When we compare stress criteria, we use $D_{\text{max}} = 0.5$ for a similar reason. As described in the main text, we argue that this is an acceptable approximation to $D_{\text{max}} \to 1$, as it still produces viscosities significantly close to 0 so as to mimic the behavior of a material that has lost its load-bearing capacity.
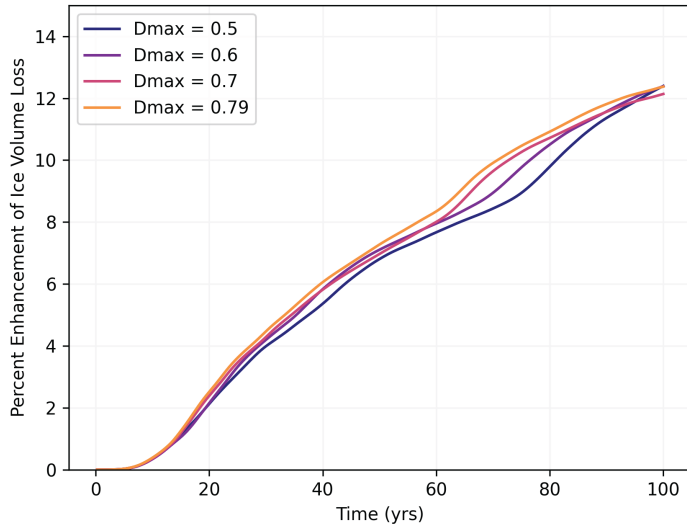
Figure S6. Estimates of ice volume loss enhancement for the case in which we compare a model run with damage initialization but no evolution with a model run with damage initialization and evolution by the diagnostic damage solver, for varying $D_{\max}$ values.

Here we show that the estimates of ice volume loss presented in the study are largely insensitive to the specific value
150 of $D_{\max}$ as long as it is sufficiently large enough. Figure S6 shows results of comparing ice volume loss with and without damage evolution for varying $D_{\max}$. The percent enhancement of ice volume loss is similar for all values of $D_{\max}$, with minor differences. Between $\sim 60-80$ years, lower values of $D_{\max}$ produce slightly lower estimates of ice volume loss enhancement, though on the century-scale, the resulting enhancement of ice volume loss is the same for all values of $D_{\max}$.

8   MISMIP+ Experiment Ice1ra

155 Here we run the MISMIP+ Experiment Ice1ra, in which we simulate grounding line retreat in response to basal melt forcing for 100 years and then turn off basal melt forcing and let the grounding line advance for another 900 years. We do this for two cases: one in which we compare damage initiation and evolution to no damage modeling at all (Figure S7), and one in which we compare damage initiation and evolution to damage initiation but no evolution (Figure S8).

The first simulation initiates with no damage, and after one model timestep of $dt = 0.25$ years, there are two lobes of damage
160 that initiate near the grounding line in the margins. After 100 years of basal melting, damage accumulates to maximum across the ice shelf, with the two initial lobes connecting. In reality, this would initiate a calving event. However, given that this model does not simulate calving currently, once basal melt forcing was turned off, that damage field advects away and, given that there is no longer climate forcing, much less damage accumulates in its place. Therefore, by 1000 years, the damage field remains again concentrated in the margins, with low damage in the center of the ice shelf.

10
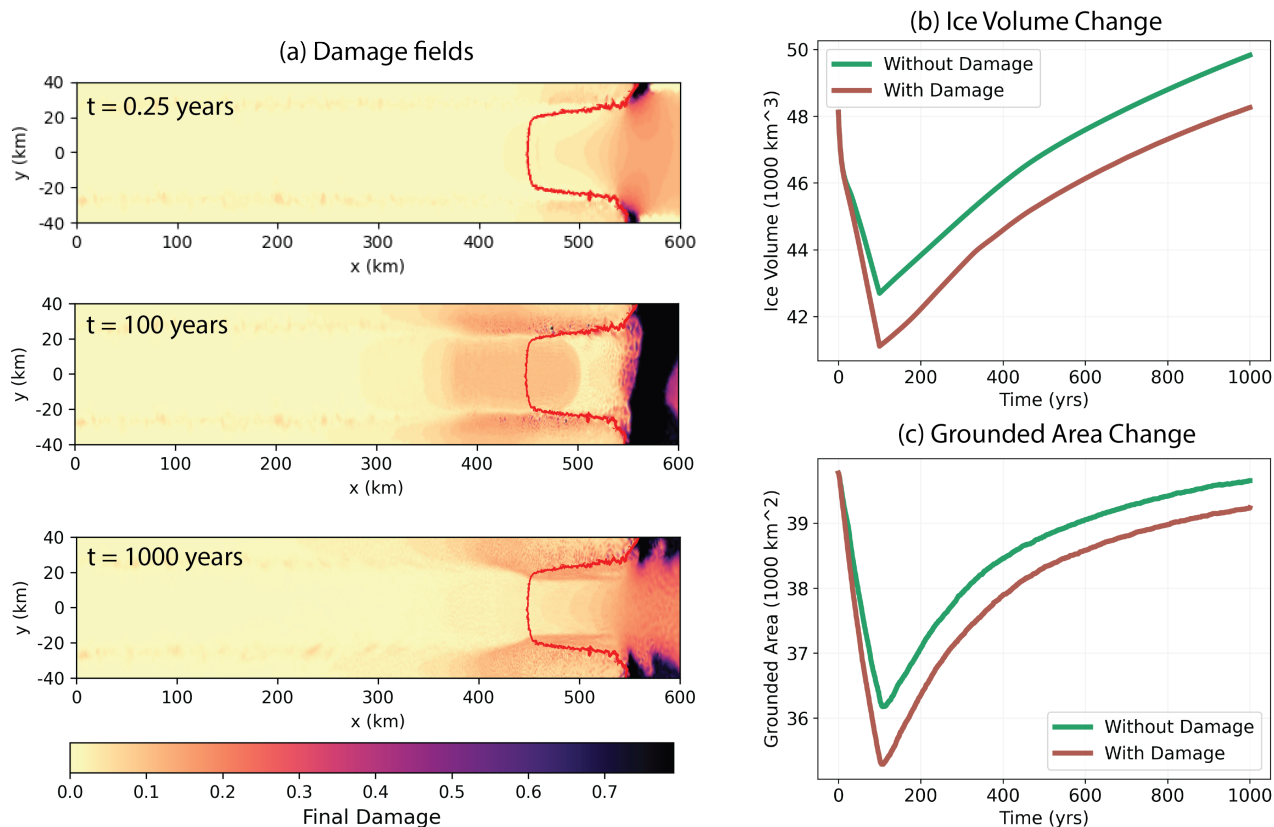
Figure S7. Results from a 1000-year simulation of the MISMIP+ model configuration for two simulations, one with damage initiation and evolution and one without, for Ice1ra experiment. (a) Damage fields at $t = 0.25, 100, 1000$ years with damage initiation and evolution, (b) Change in total ice volume over the 1000 year simulation, (c) Change in grounded area of the glacier over the 1000 year simulation.

165   However, the ice shelf does not completely recover to its previous undamaged state. This is reflected in the change in ice volume and grounded area. While the simulation with no damage largely recovers to the grounded area and ice volume of the initial steady state (in fact, with the glacier growing in volume slightly as compared to the initial state; Figure S7b), if we include damage initiation and evolution, the glacier no longer reaches its initial grounded area (Figure S7c). This suggests that damage affects the ability of the glacier to recover from grounding line retreat.

170   Next, we consider the effect of initializing a model with damage but not evolving damage (Figure S8). Initially, there is elevated damage in the margins. In response to basal melting for 100 years, damage accumulates in the margins and along the grounded ice. Once basal melting turns off, the damage field largely reverts back to its steady-state, with a few regions of elevated damage along the margins of the grounded ice (Figure S8a). Unlike the previous simulation, initializing the model with damage produces a similar behavior in grounding line advance and ice volume recovery. Both simulations do not fully

175   recover in ice volume to the initial steady-state or the initial grounded area (Figure S8b-c).
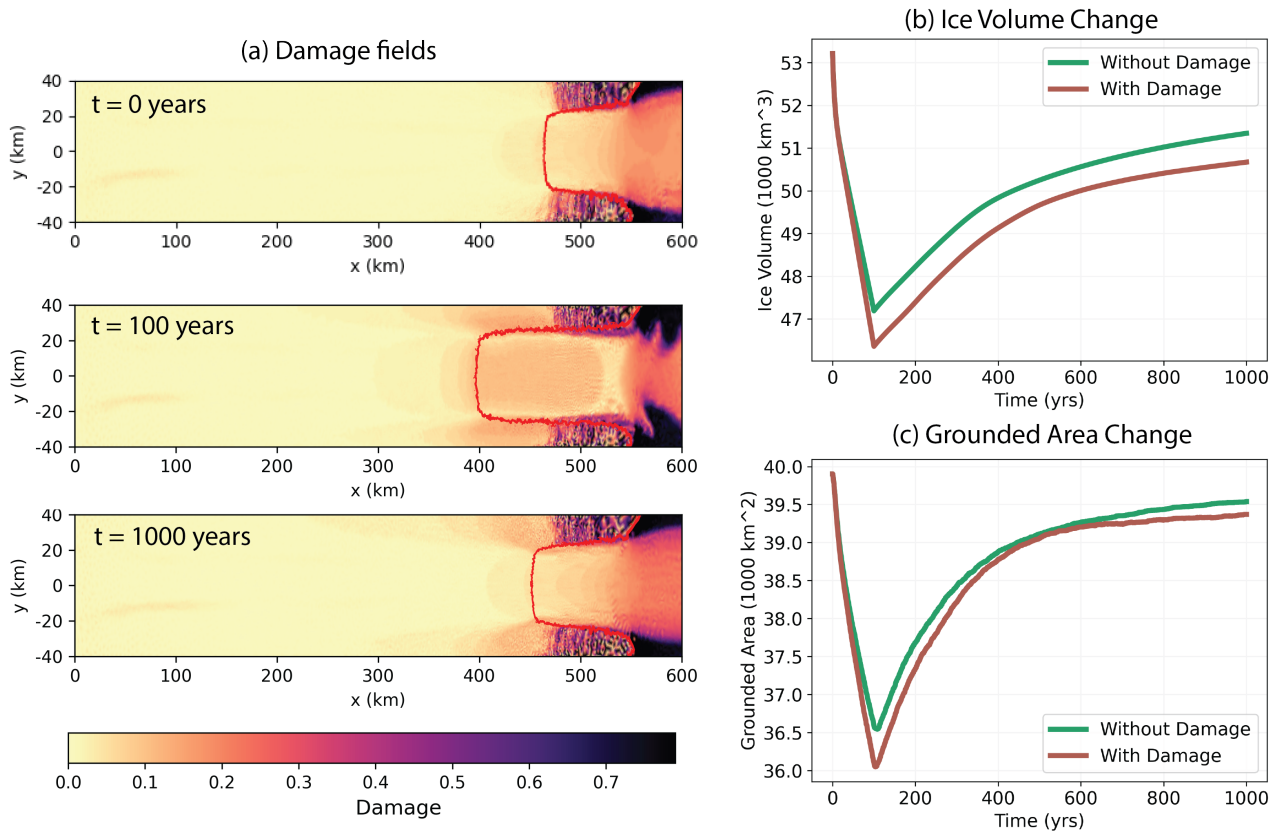
Figure S8. Results from a 100-year simulation of the MISMIP+ model configuration for two simulations, one with damage initiation but no evolution and one with both damage initiation and evolution, for Ice1ra experiment. (a) Damage fields at $t = 0, 100, 1000$ years with damage initiation and evolution, (b) Change in total ice volume over the 1000 year simulation, (c) Change in grounded area of the glacier over the 1000 year simulation.

9 MISMIP+ Experiment: Run to 500 years

In the main text, we show ice sheet response to basal melt forcing over 100 years. Here, we show how these results change if we were to run the experiments for 500 years. In Figure S9, we are comparing two simulations: one in which we initialize and evolve damage ("With Damage"), and one in which we only initialize but do not evolve damage ("Without Damage").

180   There is significant damage evolution in the margins, near the terminus, and in the center of the ice shelf (Figure S9a). Over 500 years, the effect of damage continues to enhance ice volume and grounded area loss, with the enhancement of ice volume loss $\sim 17.5\%$ by 500 years (Figure S9b-c).
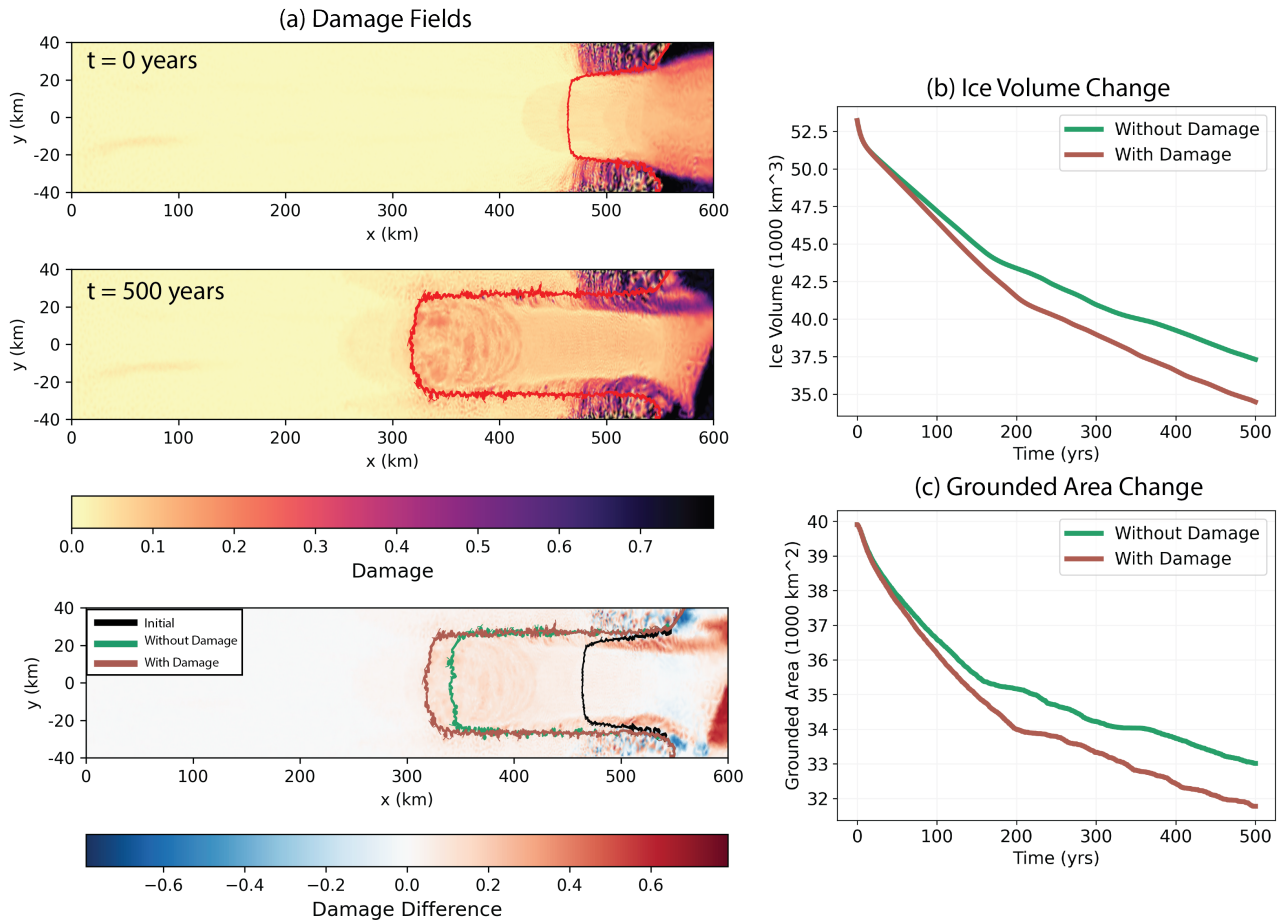
Figure S9. Results from a 500-year simulation of the MISMIP+ model configuration for two simulations, one with damage initiation but no evolution and one with both damage initiation and evolution. (a) Damage field at the beginning of the simulation (top row), after 500 years (middle row), and the difference between the two (bottom row). The bottom row also shows grounding line positions initially (black line), and after 500 years for the case without damage evolution (green line) and with damage evolution (red line). (b) Change in grounded ice area over the 500 year simulation, (c) Change in total ice volume of the glacier over the 500 year simulation.
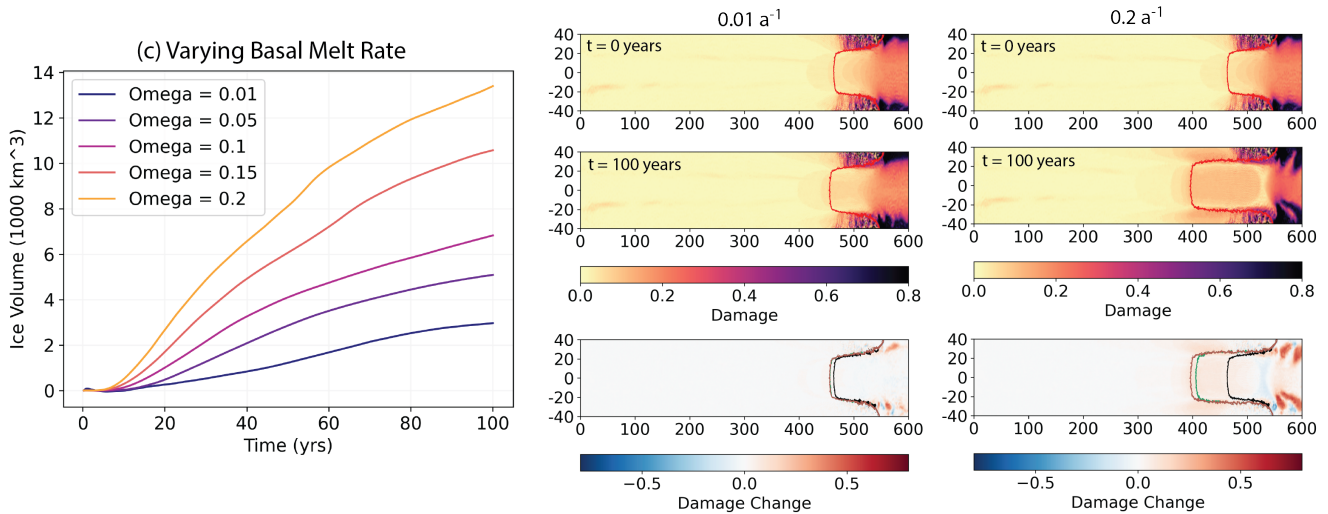
Figure S10. Effect of damage on ice volume loss for varying basal melt rate: Results from a 100-year simulation for $\Omega = 0.01, 0.05, 0.1, 0.15, 0.2 \text{ yr}^{-1}$. We show the percent enhancement of ice volume loss (difference in ice volume loss between a simulation with damage evolution and a simulation with damage initialization but no evolution as a percentage of total ice volume loss in the damage initialization simulation) and the damage fields (initial and final damage, and total damage change) for $\Omega = 0.01, 0.2 \text{ yr}^{-1}$.

10   Effect of Basal Melting Rate

The idealized glaciers in these simulations are responding to basal melt forcing as described by the chosen melt parame-
185   terization. The magnitude of basal melting is controlled by the parameter Ω, which is set to $\Omega = 0.2 \text{ yr}^{-1}$ for the MISMIP+
experiments. Here, we evaluate how changing the basal melt forcing affects the significance of damage to ice flow (Figure S10).
As Ω, and thus the basal melt rate, increases, the enhancement of ice volume loss due to damage increases, with $\Omega = 0.2$ pro-
ducing 12% enhancement and $\Omega = 0.01 \text{ yr}^{-1}$ producing 3% enhancement. This suggests the existence of a feedback between
basal melting and damage evolution, in which increased basal melting causes local thinning on the ice shelf, enhancing the
190   damage locally. This damage affects flow over the ice shelf as the damage advects downstream. This may suggest that regions
that experience strong climate forcing may be most vulnerable to damage-induced flow enhancement and thus incorporating
damage models into simulations of those regions is necessary to capture the full effect of ocean-induced melt forcing.

References

Christian, J. E., Robel, A. A., and Catania, G.: A probabilistic framework for quantifying the role of anthropogenic climate change in marine-terminating glacier retreats, The Cryosphere, 16, 2725–2743, https://doi.org/10.5194/tc-2021-394, 2022.

Huth, A., Duddu, R., and Smith, B.: A Generalized Interpolation Material Point Method for Shallow Ice Shelves. 2: Anisotropic Nonlocal Damage Mechanics and Rift Propagation, Journal of Advances in Modeling Earth Systems, 13, https://doi.org/10.1029/2020MS002292, 2021.

Keller, A. and Hutter, K.: Conceptual thoughts on continuum damage mechanics for shallow ice shelves, Journal of Glaciology, 60, 685–693, https://doi.org/10.3189/2014JoG14J010, 2014.

Pralong, A. and Funk, M.: Dynamic damage model of crevasse opening and application to glacier calving, Journal of Geophysical Research, 110, B01 309, https://doi.org/10.1029/2004JB003104, 2005.

Robel, A. A., Schoof, C., and Tziperman, E.: Rapid grounding line migration induced by internal ice stream variability, Journal of Geophysical Research: Earth Surface, 119, 2430–2447, https://doi.org/10.1002/2014JF003251, 2014.

Schoof, C.: Ice sheet grounding line dynamics: Steady states, stability, and hysteresis, Journal of Geophysical Research, 112, F03S28, https://doi.org/10.1029/2006JF000664, 2007.

Sun, S., Cornford, S. L., Moore, J. C., Gladstone, R., and Zhao, L.: Ice shelf fracture parameterization in an ice sheet model, The Cryosphere, 11, 2543–2554, https://doi.org/10.5194/tc-11-2543-2017, 2017.